Third cumulant of the total transmission of diffuse waves

M. C. W. van Rossum, Johannes F. de Boer, and Th. M. Nieuwenhuizen
Van der Waals-Zeeman Laboratorium, Universiteit van Amsterdam, Valckenierstraat 65, 1018 XE Amsterdam, The Netherlands
(Received 30 December 1994)

The probability distribution of the total transmission is studied for waves multiply scattered from a random, static configuration of scatterers. A theoretical study of the second and third cumulants of this distribution is presented. Within a diagrammatic approach a theory is developed that relates the third cumulant normalized to the average $\langle\langle T_a^3\rangle\rangle$ to the normalized second cumulant $\langle\langle T_a^2\rangle\rangle$. For a broad Gaussian beam profile, it is found that $\langle\langle T_a^3\rangle\rangle = \frac{16}{5}\langle\langle T_a^2\rangle\rangle^2$. This is in good agreement with data of optical experiments.

PACS number(s): 42.25.Bs, 78.20.Dj, 72.15.−v

I. INTRODUCTION

Multiple scattering in disordered systems is a field of wide interest; it is studied in electronic, microwave, and optical systems. In the multiple scattering regime the main transport in transmission is through diffusion. Yet interference processes, possible by the underlying wave character, play an important role. This interference leads to interesting effects such as the enhanced backscatter cone [1–3], short- and long-range correlations [4–8], and strong localization. If interference occurs between diffusion paths, it causes large fluctuations. Most famous are the sample-to-sample fluctuations in the conductance of electronic systems, the so-called universal conductance fluctuations [9–11], but also other transmission quantities are influenced by interference.

Recently, attention has been drawn not only to the variance of the fluctuations, but to all the distribution functions. Examples are the intensity distribution in speckle patterns for classical waves [12,13] and the conductance distribution for electronic systems [14]. The size of the fluctuations and the shape of the distribution are related to the "distance" from the localization transition. Far from localization, diffusion channels are almost uncorrelated and fluctuations are small (except for the optical speckle pattern in the angular resolved transmission). The correlation between the channels increases if the localization is approached. The relevant parameter is the inverse dimensionless conductance $1/g$, which can be interpreted as the chance that two channels interfere. The dimensionless conductance can be expressed in the thickness of the sample L, the mean free path ℓ, and the number of channels N,

$$g = \frac{4N\ell}{3L}. \tag{1}$$

The number of channels is calculated in analogy with a waveguide, where it is unambiguously defined. In the diffuse mesoscopic regime g^{-1} will be a small parameter of our perturbation theory (experimentally this proved to be fully justified, as there $g \sim 10^3$ [15]). Close to Anderson localization g approaches unity and fluctuations increase. The central question is how the distributions change as the strong localization regime is approached [14,16].

Let us briefly review some characteristics of optical transmission distribution functions in the regime of moderate g. In the study of mesoscopic systems using light scattering, one takes a small sample with static scatterers. In order to average, one needs to sum over a large number of scatterer configurations. In practice this is done by varying an external parameter such that the interference pattern is completely changed, whereas in electronic systems it is common to vary the Fermi energy or apply a magnetic field; in optics one usually varies the wavelength of the light. In contrast to electronic systems, not only the conductance but three different transmission quantities can be measured in optical systems. (An exception is the very recent observation of electron speckle by Gao *et al.* [17].) First, the angular resolved transmission can be considered. If a laser shines on the sample, a speckle pattern is seen in the transmission. If one measures the intensity in an outgoing direction b, this corresponds to measuring the angular transmission coefficient T_{ab}, where a denotes the incoming and b the outgoing channel. The intensities in the speckle pattern have in zeroth order in g an exponential distribution

$$P(T_{ab}) = \frac{1}{\langle T_{ab}\rangle} \exp\left(-\frac{T_{ab}}{\langle T_{ab}\rangle}\right), \tag{2}$$

which is also known as the Rayleigh law. Deviations from this law occur if interference between the transmitted intensities, the diffuson propagators, is taken into account: the higher moments of the distribution function increase. For large values of the transmission a stretched exponential was observed [12], which was recently predicted as [16] $P(T_{ab}) \propto \exp(-2\sqrt{gT_{ab}/\langle T_{ab}\rangle})$.

One obtains another transmission quantity if one collects all the outgoing light and also all incoming directions are used, i.e., using a diffuse incoming wave instead of a plane wave. In this case one sums over all incoming and outgoing channels and the conductance of the

sample $g = \sum_{a,b} T_{ab}$ is measured. It corresponds to the well known conductance measurement for electron systems. The conductance has roughly a Gaussian distribution. The absolute variance is larger than expected classically because of interference and it does not depend on the sample parameters (hence the name universal conductance fluctuations) [9–11]. Equivalently, the relative variance is proportional to g^{-2}. The full distribution function of the conductance was studied by Altshuler, Kravtsov, and Lerner [14], who predict a log-normal tail for the tail of the distribution function. For the lower cumulants they predict that $\langle g^n \rangle_{\rm cum} \propto \langle g^{2-n} \rangle$. Note, however, that the prefactors maybe zero, as Macêdo [18] found that $\langle g^3 \rangle_{\rm cum} \propto \langle g \rangle^{-2}$.

We are, however, interested in yet another transmission quantity. It is obtained by spatially integrating the speckle pattern on the outgoing side and taking an incoming plane wave. One thus obtains an intermediate quantity between the angular transmission T_{ab} and the conductance $\sum_{a,b} T_{ab}$. It is termed the total transmission $T_a = \sum_b T_{ab}$. This quantity is the subject of this paper. The total transmission is a constant superposed with fluctuations. In first order of g^{-1} the fluctuations have a Gaussian distribution [8,13]. The relative variance of this distribution is proportional to g^{-1}; it is thus a factor g larger than for the conductance fluctuations. This sensitivity of the total transmission to interference processes and its simple limiting behavior (as compared to the angular resolved transmission) make it an ideal quantity to study mesoscopic transmission. Its full distribution was studied numerically in two dimensions by Edrei, Kaveh, and Shapiro, who recovered the Gaussian distribution function, tending towards a log-normal distribution near the Anderson transition [19]. The full distribution function was recently derived [16]. It was shown that it has a log-normal distribution growth and an exponential tail.

Recently the third cumulant of the distribution was found experimentally by de Boer *et al.* [15]. In this paper we present the theoretical details of that work. We focus on the Gaussian distribution and the deviation from the Gaussian due to the presence of the third cumulant. The structure of this paper is as follows. The diffusion in optical systems is described in Sec. II. In Sec. III the character of the probability distribution is discussed. In Sec. IV we calculate the second and in Secs. V and VI we calculate the third cumulant of the probability distribution. Next we calculate experimental corrections to our result in Secs. VII and VIII, after which we compare our results with the experimental data in Sec. IX. We close with a discussion in Sec. X.

II. DIFFUSE TRANSPORT

Consider the transport of light through a three-dimensional slab with static scatterers in a random configuration. The slab has a thickness L. The diffuse mesoscopic regime is characterized by $\lambda \ll \ell \ll L$. Here ℓ denotes the mean free path and λ denotes the wavelength in the medium. Isotropic scattering is assumed. We also work in the scalar wave approximation. It is known that the two independent polarization directions of light effectively double the number of channels N in the problem as compared to the scalar wave case [8]. Apart from a small correction term, our final result does not depend on the number of channels and the doubling.

We take the depth in the the slab as the z coordinate; the slab thus corresponds to $0 < z < L$. A plane scalar wave with unit flux and area A impinges on the sample from direction a. It is given by

$$\psi^a_{\rm in}(\mathbf{r}) = \frac{1}{\sqrt{Ak\mu_a}} \exp(iP_a R + ik\mu_a z), \qquad z < 0, \quad (3)$$

where k is the wave number, $R = (x, y)$ is the transversal coordinate, P_a is the transverse component of the momentum, and $\mu_a = \sqrt{1 - P_a^2/k^2} = \cos\theta_a$, where θ_a is the angle with respect to the z axis. The number of channels depends on the area of the incoming beam. Dividing the total area of the beam with diameter ρ_0 in small coherence regions of area λ^2, one obtains in analogy with waveguides $N = 2k^2\rho_0^2/4$, or the Weyl formula $N = 2k^2A/4\pi$. The factor $it2$ comes from the two independent polarization directions. For the case of scalar wave scattering this doubling factor should be left out. The main contribution to the average transmission is given by the diffuse transport of intensity. This means that the two amplitudes, which make up the intensity, scatter on the same scatterers following the same path through the sample. In diagrammatic language these processes are known as diffuson propagators or ladder diagrams. An example of such a scattering process is drawn in Fig. 1; in the following we will depict the diffuson propagators by close parallel lines and omit the scatterers for clarity.

In the bulk the diffuse intensity obeys simply the diffusion equation, but the precise prefactors from the coupling to the outside have to be determined from the Schwarzschild-Milne equation [20]

$$\mathcal{L}(z) = S(z) + \int_0^L dz' M(z, z') \mathcal{L}(z'). \quad (4)$$

This is a self-consistent transport equation that gives the diffuse intensity $\mathcal{L}$ resulting from a source S. The ker-

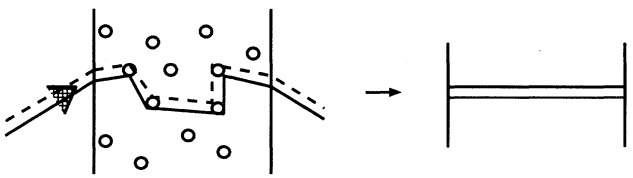

FIG. 1. Left: an example of an actual scattering process; a retarded (full line) and an advanced amplitude (dashed line) come from the left and share the same path through the sample. Right: schematic representation of the average process, the diffuson propagator (for clarity the scatterings are not drawn).

nel M describes the intensity decay between two scatterings. In the ladder approximation (without internal reflections) it is

$$M(z,z') = \int_0^1 \frac{d\mu}{2\mu} e^{-|z-z'|/\mu\ell}. \tag{5}$$

The source term S is given by the single scattered incoming intensity. Our incoming plane wave leads to a source in the Milne equation

$$S(z) = nt\bar{t}|\Psi^a_{\rm in}|^2 = \frac{4\pi}{Ak\mu_a\ell} \exp[-z/(\mu_a\ell)], \tag{6}$$

where n is scatterer density and t is the t matrix, giving the mean free path $\ell = 4\pi/(nt\bar{t})$. The transport equation (4) now yields for an incoming diffuson propagator

$$\mathcal{L}^a_{\rm in}(z) = \frac{4\pi\tau_1(\mu_a)}{k\ell A\mu_a} \frac{L-z}{L}, \tag{7}$$

where τ_1 describes the limit intensity of a semi-infinite system; see Ref. [21].

Now that the prefactors are known, we continue with the diffusion equation, which holds a few mean free paths away from the surface. We generalize to the case where the amplitudes making up the diffuson propagator have a nonzero momentum. For the corresponding diffusion propagator propagating from point z to point z' it holds that

$$\begin{aligned} -\nabla^2\mathcal{L}^{\rm int}(z,z') &= -\partial_z^2\mathcal{L}^{\rm int}(z,z') + Q^2\mathcal{L}^{\rm int}(z,z') \\ &= \frac{12\pi}{\ell^3}\delta(z-z'), \end{aligned} \tag{8}$$

with approximate boundary conditions $\mathcal{L}^{\rm int}(0,z';Q) = \mathcal{L}^{\rm int}(L,z';Q) = 0$. Here Q is a two-dimensional vector, defined as the difference of perpendicular momenta of the two incoming amplitudes making up the diffuson propagator. If coherent waves impinge with a different angle on the sample, this net transverse momentum of diffuson propagators need not be zero and the diffuson propagators decay exponentially with the inverse decay length equal to $|Q|$. The solution of the diffusion equation reads

$$\mathcal{L}^{\rm int}(z,z';Q) = \frac{12\pi}{\ell^3} \frac{\sinh(|Q|z_<)\sinh[|Q|(L-z_>)]}{|Q|\sinh(|Q|L)}, \tag{9}$$

with $z_< = \min(z,z')$ and $z_> = \max(z,z')$. Below we also need incoming diffuson propagators with transverse momenta, which are obtained by combining the prefactor of Eq. (7) with the $z_>$ dependence of Eq. (9).

The total transmission is obtained by integrating over the outgoing channels. In the experimental geometry of Ref. [15], the outgoing radiation was collected in an integrating sphere. Only outgoing diffuson propagators where their amplitudes are exactly in phase (i.e., have opposite phase) are leading after this integration. Therefore the outgoing diffuson propagator can have no transverse momentum. The transport equation (4) yields an outgoing diffuson propagator from a unit source

$$\mathcal{L}_{\rm out} = \frac{k}{\ell}\frac{z}{L}. \tag{10}$$

The total transmission is obtained by connecting the incoming to the outgoing diffuson propagator, as shown in Refs. [21,22],

$$\langle T_a\rangle = 2\frac{\tau_1(\mu_a)\ell}{3L\mu_a}. \tag{11}$$

Here we included the doubling from the two polarization directions. Also integrating over all incoming directions yields the conductance [22]

$$g = \sum_a \langle T_a\rangle = 2\frac{\ell k^2 A}{3\pi L}; \tag{12}$$

with $N = 2k^2A/4\pi$ this equals our previous definition (1).

III. CUMULANTS OF THE PROBABILITY DISTRIBUTION

In this section we introduce the probability distribution of the total transmission of scalar waves and we discuss some of its properties. The corrections for vector waves will be made in Sec. VIII. We will link the moments of the distribution to diagrams. The moments of the probability distribution $P(T_a)$ can be extracted as

$$\langle T_a^k\rangle = \int dT_a\, P(T_a) T_a^k. \tag{13}$$

In a diagrammatic approach the kth moment can be represented by a diagram with k diffuson propagators on both the incoming and the outgoing side. The $k=1$ term is the average total transmission $\langle T_a\rangle$, as given by the Schwarzschild-Milne equation in Eq. (11). This quantity is given by a single diffuson propagator and is thus independent of channel-to-channel correlations. The second moment can be decomposed in the first two cumulants

$$\frac{\langle T_a^2\rangle}{\langle T_a\rangle^2} = \frac{\langle T_a\rangle^2 + \langle T_a^2\rangle_{\rm cum}}{\langle T_a\rangle^2} = 1 + \langle\langle T_a^2\rangle\rangle. \tag{14}$$

The double angular brackets denote cumulants normalized to the average. Diagrammatically the second moment is depicted in Fig. 2. The decomposition in cumulants will prove useful as each cumulant corresponds to a different number of interactions between the diffuson propagators. In the first term [Fig. 2(a)] there is no interference; it factorizes in the average transmission squared (apart from a small correction discussed in Sec. VIII). The second term [Fig. 2(b)] is the second cumulant $\langle\langle T_a^2\rangle\rangle$. It gives the variance of the fluctuations. Interactions between two diffuson propagators are responsible for the presence of this second cumulant. The interference process is, in diagrammatic language, the so-called Hikami box, depicted as the shaded square in Fig. 2(b). In the box two amplitudes of the incoming

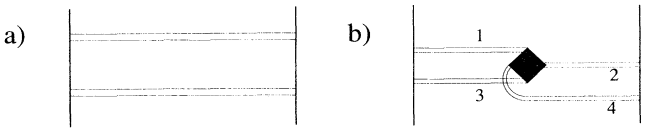

FIG. 2. Two contributions to the second moment of the total transmission. In diagram (a) the transmission channels are independent; this process is of order unity and is almost completely reducible to the mean value squared. Diagram (b) corresponds to two interfering channels. This is the second cumulant; it is of order $1/g$. The close parallel lines are diffuson propagators; the shaded square denotes the Hikami four-point vertex.

diffuson propagators are interchanged, causing a correlation between the outgoing ones. Precisely the same process was studied in the more general context of the long-range correlation functions [23–26]. In the work of de Boer, van Albada, and Lagendijk [8] and Garcia *et al.* [7] the correlation between two diffuson propagators with different frequency was measured. This is the so-called C_2 correlation function $C_2(\Delta\omega) = \langle\langle T_a(\omega)T_a(\omega+\Delta\omega)\rangle\rangle$. For our case we find that $\langle\langle T_a^2\rangle\rangle = C_2(0)$, which thus corresponds to the peak value of this correlation function. In Sec. IV we will calculate this cumulant in detail.

Similarly to the second moment, one can distinguish three different contributions to the third moment

$$\frac{\langle T_a^3\rangle}{\langle T_a\rangle^3} = 1 + 3\langle\langle T_a^2\rangle\rangle + \langle\langle T_a^3\rangle\rangle. \tag{15}$$

The corresponding leading diagrams are drawn in Fig. 3. The first term [Fig. 3(a)] again corresponds to the transmission without interference. The second term [Fig. 3(b)] is reducible in a single diffuson propagator and a second cumulant diagram. From the figure it is clear that this decomposition can be done in three ways, which is reflected in the prefactor of $\langle\langle T_a^2\rangle\rangle$ in Eq. (15). The third

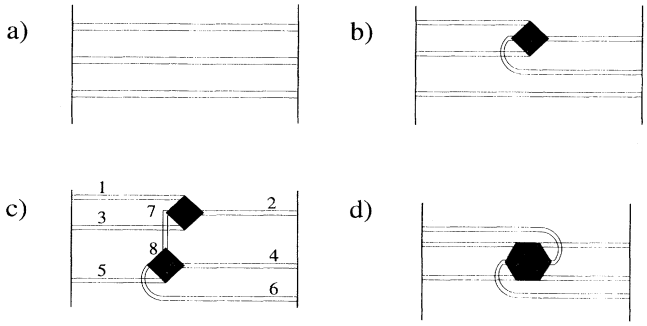

FIG. 3. Three contributions to the third moment of the total transmission. Diagram (a) corresponds to independent transmission channels; it is of order 1. In diagram (b) there is correlation but it can be decomposed into the second cumulant; this is of order g^{-1}. Diagrams (c) and (d) are the contributions to the third cumulant, $O(g^{-2})$.

contribution stands for the third cumulant in the distribution and expresses the leading deviation from the Gaussian distribution. This is the term we are mainly interested in. It consists of two related diagrams: Figs. 3(c) and 3(d). The three intensities can interfere twice two by two or the intensities can interact all three together with a so-called Hikami six-point vertex. Both contributions will prove to be of the same order of magnitude. The strength of the effect can be easily estimated using the interpretation of $1/g$ as an interaction probability. By looking at the diagram, the third cumulant is proportional to the chance of two diffuson propagators meeting twice, thus of order $1/g^2$. We find the basic result

$$\langle\langle T_a^3\rangle\rangle \propto \langle\langle T_a^2\rangle\rangle^2. \tag{16}$$

The rest of the paper essentially consists of proving this relation and determining the prefactor. Finally, we will compare this relation to the experimental data of Ref. [15].

Because only a limited number of channels is sampled in an experiment, the law of large numbers predicts a distribution with some nonzero width even if we only consider disconnected diagrams. However, we will show in Sec. VIII that this effect brings only a negligible contribution to the measured cumulants. The large fluctuations are due almost entirely to the interference.

Note that in our calculations diagrams with loops are neglected. An example of a loop diagram is the C_3 (or universal conductance fluctuation) contribution to the second cumulant [10,6,22]. One of the C_3 diagrams is a second cumulant diagram where the outgoing diffuson propagators are again input for another Hikami box. (It is like gluing two second cumulant diagrams one after the other.) This diagram contains two Hikami boxes; therefore it gives a contribution of order g^{-2} to the second cumulant. In general, one easily sees that in order to create a loop, one needs a higher number of interference vertices. Therefore, these diagrams are of higher order in $1/g$ and we did not calculate them. The leading contributions to the cumulants are by far sufficient for the description of the experiment of Ref. [15].

IV. THE SECOND CUMULANT

In this section we recover the results for the second cumulant. This quantity was often calculated in literature. In the work of the Boer, van Albada, and Lagendijk [8] the frequency correlation in the total transmission was calculated using a Langevin approach introduced by Spivak and Zyuzin [24]; see also the work of Pnini and Shapiro [23]. Here we obtain the same results using a diagrammatic technique [6,4,27]. We calculate the diagram of Fig. 2(b). The interaction vertex of the diffuson propagators is the Hikami four-point vertex or Hikami box [28]. The Hikami box is depicted in Fig. 4. From the figure it is easily seen that the vertex interchanges two amplitudes of the incoming diffuson propagators. As shown, the full vertex is (in the second-order Born approximation) the sum of one bare vertex and two vertices with an addi-

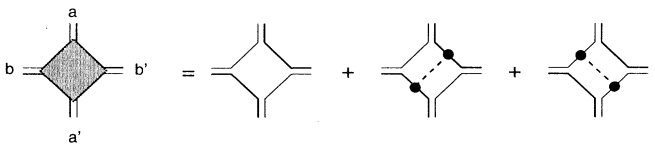

FIG. 4. Hikami four-point vertex. It describes the exchange of amplitudes of two incoming diffuson propagators a and a' into two outgoing diffuson propagators b and b'. The dots linked with the dashed line denote the dressing with an extra scatterer.

tional scatterer. (If the scatterers are near resonance, the second-order Born approximation is no longer valid and more diagrams are relevant. However, for the four-point vertex it was explicitly proven in Ref. [29] that this will only be reflected in the different value of the mean free path.) The summation of the diagrams yields [28,30]

$$H_4 = \frac{-\ell^5}{48\pi k^2}\left[\mathbf{q}_a\cdot\mathbf{q}_{a'} + \mathbf{q}_b\cdot\mathbf{q}_{b'} - \frac{1}{2}(\mathbf{q}_a^2 + \mathbf{q}_{a'}^2 + \mathbf{q}_b^2 + \mathbf{q}_{b'}^2)\right]. \quad (17)$$

To this vertex two incoming diffuson propagators a and a' and two outgoing diffuson propagators b and b' are attached. The $\mathbf{q}_i$ denotes the *three-dimensional* momentum of the corresponding diffuson. The momenta are pointing toward the vertex. For our second cumulant diagram of Fig. 2(b) we have numbered $a = 1$, $a' = 3$, $b = 2$, and $b' = 4$.

As stated above, only the outgoing diffuson propagators where the amplitudes have exactly opposite phase are leading in the total transmission measurements. Therefore the transversal momenta of the outgoing diffuson propagators must be zero $Q_2 = Q_4 = 0$, but as amplitudes are exchanged in the Hikami box, the incoming diffuson propagators can have a transversal component in their momentum. Using momentum conservation one has $Q_1 = -Q_3 \equiv Q$.

After Fourier transforming Eq. (17) in the z coordinate we find

$$H_4 = \frac{\ell^5}{48\pi k^2}\left(\partial_{z_1}\partial_{z_3} + \partial_{z_2}\partial_{z_4} - Q_1\cdot Q_3 - \frac{1}{2}\sum_{i=1}^{4}(\partial_{z_i}^2 - Q_i^2)\right). \quad (18)$$

Here ∂_{z_1} stands for differentiating toward the z coordinate of the diffuson propagator with the same number, in this case $\mathcal{L}_1(z)$. The terms inside the sum in Eq. (18) are neglected. According to the diffuson propagator equation, they yield approximately a source term near the boundary of the sample. In the integral these contributions are of the negligible order. In the plane wave limit of the incoming beam, all transverse momenta are absent and the diffuson propagators are simple linear functions, given by Eqs. (7) and (10). One obtains the known result for the second cumulant [4]

$$\langle\langle T_a^2\rangle\rangle = \langle T_a\rangle^{-2}\int\int dxdy \times\int_0^L dz H_4\mathcal{L}_1(z)\mathcal{L}_2(z)\mathcal{L}_3(z)\mathcal{L}_4(z) = \frac{1}{gL^3}\int_0^L dz[z^2 + (1-z)^2] = \frac{2}{3}g^{-1}. \quad (19)$$

Taking only this second cumulant we find for the moment a Gaussian probability distribution in the plane wave limit [13]

$$P(T_a) = \sqrt{\frac{3g}{4\pi}}\exp\left[-\frac{3g}{4}\left(T_a - \langle T_a\rangle\right)^2\right]. \quad (20)$$

Let us now study the influence of the beam profile on the correlation. If the spot of the incoming beam is finite, amplitudes with different transverse momenta are present. They can combine into incoming diffuson propagators with a perpendicular momentum. We suppose that the incoming beam has a Gaussian profile. It is decomposed into plane waves defined in Eq. (3) (for convenience we assume perpendicular incidence)

$$\psi_{\text{in}} = \frac{2\pi}{W}\sum_a \phi(Q_a)\psi_{\text{in}}^a, \qquad \phi(Q) = \frac{\rho_0}{\sqrt{2\pi}}e^{-Q^2\rho_0^2/4}, \quad (21)$$

where ρ_0 is the beam diameter. In order to have two diffuson propagators with a momenta Q and $-Q$, we find that the four incoming amplitudes combine to a weight function

$$\int d^2P_1 d^2\ P_3\ \phi(P_1)\phi^*(P_1+Q)\ \phi(P_3)\phi^*(P_3-Q) = e^{-\rho_0^2Q^2/4}. \quad (22)$$

The second cumulant is now found by first calculating the Q-dependent correlation. This is done similarly to the calculation above, but now the $Q_1\cdot Q_3$ terms in Eq. (18) should be taken into account, as well as the Q dependence of the incoming diffuson propagators; see Eq. (9). (The outgoing diffuson propagators still have no such momentum.) The total cumulant is now found by integrating over the momentum with the corresponding weight. For a Gaussian beam profile one finds [8]

$$\langle\langle T_a^2\rangle\rangle = \frac{\rho_0^2}{4\pi g}\int d^2Q\, e^{-\rho_0^2Q^2/4}F_2(|Q|L), \quad (23)$$

with $F_2(x) = [\sinh(2x) - 2x]/[2x\sinh^2 x]$. If the incoming beam is again very broad, $\rho_0 \gg L$, only the term $F_2(|Q|L = 0) = 2/3$ contributes and one recovers the plane wave behavior $\langle\langle T_a^2\rangle\rangle = 2/3g$. Note that this agreement is found by identifying the area of a Gaussian profile with $A = \pi\rho_0^2$. This definition is somewhat arbitrary and other choices are also possible [16]. After fixing this definition, no freedom remains and we will see that for the

third cumulant a Gaussian profile leads to results other than a plane wave.

The second cumulant decreases as $1/\rho_0^2$ at large ρ_0. In a real space picture it is evident that the correlation increases if the two incoming channels are closer to each other, i.e., if the beam diameter is smaller. In the experiment of Ref. [15] the focus was kept small in order to minimize the dimensionless conductance g and therefore to maximize the fluctuations.

V. THE THIRD CUMULANT

We now discuss the calculation of the third cumulant. As mentioned, there are two processes contributing: one with two four-point vertices, which we term $\langle\langle T_a^3\rangle\rangle_c$, and one with a six-point vertex $\langle\langle T_a^3\rangle\rangle_d$, where we have chosen the subscript according to Fig. 3. This process was, to our knowledge, not studied before. Our calculation follows the lines of the second cumulant calculation.

A. Interference via two four-point vertices

First consider the diagram in Fig. 3(c). We have labeled incoming diffuson propagators with odd numbers, the outgoing ones with even numbers. Two incoming diffuson propagators $\mathcal{L}_1$ and $\mathcal{L}_3$ meet at a position z. In a Hikami box the diffuson propagator $\mathcal{L}_1$ interferes with $\mathcal{L}_3$, forming $\mathcal{L}_2$ and an internal diffuson propagator $\mathcal{L}_{78}^{\rm int}$. The $\mathcal{L}_2$ propagates out, whereas $\mathcal{L}_{78}^{\rm int}$ interferes again at z' with incoming diffuson propagator $\mathcal{L}_5$ into two outgoing ones $\mathcal{L}_4$ and $\mathcal{L}_6$. Apart from this process, three other sequences of interference are also possible. This means that the diffuson propagators can also be permuted as $(\mathcal{L}_1,\mathcal{L}_3,\mathcal{L}_5,\mathcal{L}_2,\mathcal{L}_4,\mathcal{L}_6) \to (\mathcal{L}_3,\mathcal{L}_5,\mathcal{L}_1,\mathcal{L}_4,\mathcal{L}_6,\mathcal{L}_2) \to (\mathcal{L}_5,\mathcal{L}_1,\mathcal{L}_3,\mathcal{L}_6,\mathcal{L}_2,\mathcal{L}_4)$. We will denote the sum over these permutations as $\sum_{\rm per}$. As the diagrams can also be complex conjugated, there is also an combinatorial factor 2 for all diagrams. (Note that complex conjugation for the *second* cumulant diagram does not yield a different diagram and thus it should not be taken into account.) The expression for the diagram of Fig. 3(c) is now

$$\langle\langle T_a^3\rangle\rangle_c = \langle T_a\rangle^{-3}\, 2\sum_{\rm per} A\int_0^L dz\int_0^L dz'\; H_4(z)H_4(z') \times\mathcal{L}_1(z)\mathcal{L}_2(z)\mathcal{L}_3(z)\mathcal{L}_4(z')\mathcal{L}_5(z') \times\mathcal{L}_6(z')\mathcal{L}_{78}^{\rm int}(z,z'). \tag{24}$$

It turns out that it is useful to rewrite the form of the Hikami boxes as introduced in Eq. (17) into an equivalent expression, using momentum conservation $\mathbf{q}_a+\mathbf{q}_{a'}+\mathbf{q}_b+\mathbf{q}_{b'}=\mathbf{0}$. In real space the use of momentum conservation corresponds to partial integration. The Hikami box is again simplified using the fact that there are no transversal momentum terms, or Q terms, for the outgoing diffuson propagators. Also the source terms q^2 of incoming and outgoing diffuson propagators are neglected. Using the numbering in Fig. 3, we obtain

$$H_4(z) = \frac{-\ell^5}{48\pi k^2}[2\partial_{z_1}\partial_{z_2} + 2\partial_{z_2}\partial_{z_3}],$$
$$H_4(z') = \frac{\ell^5}{48\pi k^2}[2\partial_{z_4}\partial_{z_6} - \partial_{z_8}^2 + Q_8^2]. \tag{25}$$

Source terms, i.e., q_i^2 terms, of the incoming and outgoing diffuson propagators were again neglected, but the source term of the diffuson propagator between the vertices is important. As seen with the diffusion equation (8), it brings

$$\partial_{z_8}^2\mathcal{L}_{78}^{\rm int}(z,z') + Q_8^2\mathcal{L}_{78}^{\rm int}(z,z') = \frac{\ell^3}{12\pi}\delta(z-z'). \tag{26}$$

The contribution from the source term [i.e., $H_4(z') \propto -\partial_{z_8}^2 + Q_8^2$, $H_4(z) \propto \partial_{z_1}\partial_{z_2} + \partial_{z_2}\partial_{z_3}$] is

$$-\left(\frac{\ell^5}{48\pi k^2}\right)^2 4\sum_{\rm per} A\int dz(\partial_{z_1}\partial_{z_2} + \partial_{z_2}\partial_{z_3})\mathcal{L}_1\mathcal{L}_2\mathcal{L}_3 \times\int dz'(-\partial_{z_8}^2 + Q_8^2)\mathcal{L}^{\rm int}\mathcal{L}_4\mathcal{L}_5\mathcal{L}_6$$
$$= -\frac{\ell^7 A}{48\pi k^4}\int_0^L dz[\partial_{z_1}\partial_{z_2} + \partial_{z_2}\partial_{z_3} + \partial_{z_3}\partial_{z_4} + \partial_{z_4}\partial_{z_5} + \partial_{z_5}\partial_{z_6} + \partial_{z_6}\partial_{z_1}]\mathcal{L}_1\mathcal{L}_2\mathcal{L}_3\mathcal{L}_4\mathcal{L}_5\mathcal{L}_6. \tag{27}$$

Although this corresponds to a local process (just one z coordinate is involved), it is of leading order. Together with the expression coming from $H_4(z')$ proportional to $\partial_{z_4}\partial_{z_6}$, we find for the total contribution of the process in Fig. 3(c)

$$\langle\langle T_a^3\rangle\rangle_c = \langle T_a\rangle^{-3}\left(\frac{l^5}{48\pi k^2}\right)^2 8\sum_{\rm per} A\int_0^L dz\; \mathcal{L}_1(z)\mathcal{L}_2'(z)\mathcal{L}_3(z)\int_0^L dz'\; \mathcal{L}_4'(z')\mathcal{L}_5(z')\mathcal{L}_6'(z')\partial_z\mathcal{L}^{\rm int}(z,z')$$
$$-\langle T_a\rangle^{-3}\frac{\ell^7 A}{48\pi k^4}\int_0^L dz[\partial_{z_1}\partial_{z_2} + \partial_{z_2}\partial_{z_3} + \partial_{z_3}\partial_{z_4} + \partial_{z_4}\partial_{z_5} + \partial_{z_5}\partial_{z_6} + \partial_{z_6}\partial_{z_1}]$$
$$\times\mathcal{L}_1(z)\mathcal{L}_2(z)\mathcal{L}_3(z)\mathcal{L}_4(z)\mathcal{L}_5(z)\mathcal{L}_6(z), \tag{28}$$

where $\mathcal{L}'(z)$ denotes the derivative toward z of $\mathcal{L}(z)$. Calculated for a plane wave it gives

$$\langle\langle T_a^3\rangle\rangle_c = \frac{28}{15g^2}, \tag{29}$$

which is indeed proportional to g^{-2}, as predicted.

B. Contribution of the six-point vertex

There is another diagram contributing to the third cumulant that is of the same order of magnitude as the process calculated above; it is depicted in Fig. 3(d). It can be thought of in the following way: The use of the Hikami box in the preceding subsection assumes that the outgoing legs scatter at least once before they propagate out or interfere again. This is a reasonable assumption for the outgoing diffuson propagators, but for the internal diffuson propagator $\mathcal{L}_{78}^{\rm int}$ it also possible that coming from z it directly, i.e., without scattering, interferes again at z'. This process is not included in the calculation of Sec. V A but has to be studied separately. The unscattered intensity decays exponentially over one mean free path; therefore this process is only important if z and z' are within one mean free path. We denote the corresponding vertex as H_6, as six diffuson propagators are connected to this diagram. This diagram was also already calculated by Hikami [28]. Also, here, the dressings of the diagrams have to be added to the bare diagrams. Taking rotations of the depicted diagrams into account, there are 16 diagrams in the second-order Born approximation. It is not allowed to dress the bare six-point vertex (leftmost right-hand side diagram in Fig. 5) with a scatterer that connects two opposite propagators. This dressing gives also a leading contribution even if the dressing is performed with an arbitrary number of scatterers, but the resulting diagram is the same as the composed diagram with two four-point vertices [Fig. 3(c)] and thus should not be counted. Yet this observation is useful to check the combinatorial ratio between the six-point vertex and the composed diagram: the forbidden dressing can be performed in three ways. As the diagrams can also be complex conjugated, there is also a factor 2 for all diagrams.

In the lowest order of $(q\ell)$ we find for the six-point vertex

$$H_6 = \frac{-\ell^7}{96\pi k^4}\Big[\mathbf{q}_1\cdot\mathbf{q}_2 + \mathbf{q}_2\cdot\mathbf{q}_3 + \mathbf{q}_3\cdot\mathbf{q}_4 + \mathbf{q}_4\cdot\mathbf{q}_5 + \mathbf{q}_5\cdot\mathbf{q}_6 + \mathbf{q}_6\cdot\mathbf{q}_1 + \sum_i q_i^2\Big]. \tag{30}$$

Hikami's original expression can be recovered from this using momentum conservation. After a Fourier transformation in the z direction, the six-point vertex yields a contribution to the third cumulant

$$\langle\langle T_a^3\rangle\rangle_d = \langle T_a\rangle^{-3}\frac{\ell^7 A}{48\pi k^4}\int_0^L dz[\partial_{z_1}\partial_{z_2} + \partial_{z_2}\partial_{z_3} + \partial_{z_3}\partial_{z_4} + \partial_{z_4}\partial_{z_5} + \partial_{z_5}\partial_{z_6} + \partial_{z_6}\partial_{z_1}] \times\mathcal{L}_1(z)\mathcal{L}_2(z)\mathcal{L}_3(z)\mathcal{L}_4(z)\mathcal{L}_5(z)\mathcal{L}_6(z). \tag{31}$$

Here we use the fact that all outgoing diffuson propagators have zero transversal momentum. Therefore all Q_iQ_j terms are absent. In the limit of an incoming plane wave we find a contribution to the third cumulant

$$\langle\langle T_a^3\rangle\rangle_d = -\frac{4}{5g^2}. \tag{32}$$

The contribution from the source term, i.e., Eq. (27) of Sec. V A, exactly cancels the contribution from the six-point vertex. The cancellation seems plausible as one does not expect short distance properties to be important in the total process. Nevertheless, this cancellation depends on the precise form of the Hikami four-point vertex in Eq. (25). If we use other equivalent forms of the Hikami box the contributions of the single and double integral in Eq. (28) are shifted with respect to each other and a full cancellation is not present. Of course, neither the result for Eq. (28) nor the final result for $\langle\langle T_a^3\rangle\rangle$ relies on this choice. The precise mechanism behind this is not clear to us. However, using the cancellation we only need to consider the term in Eq. (28), which comes from $H_4(z) \propto \partial_{z_1}\partial_{z_2} + \partial_{z_2}\partial_{z_3}$, $H_4(z') \propto \partial_{z_4}\partial_{z_6}$, and the permutations. We thus obtain for the third cumulant

$$\langle\langle T_a^3\rangle\rangle = \langle\langle T_a^3\rangle\rangle_c + \langle\langle T_a^3\rangle\rangle_d = \langle T_a\rangle^{-3}\frac{\ell^{10}A}{288\pi^2k^2}\sum_{\rm per}\int_0^L dz\,\mathcal{L}_1(z)\mathcal{L}_2'(z)\mathcal{L}_3(z) \times\int_0^L dz'\,\mathcal{L}_4'(z')\mathcal{L}_5(z')\mathcal{L}_6'(z')\partial_z\mathcal{L}^{\rm int}(z,z'). \tag{33}$$

In the next section we calculate this expression for various incoming beam profiles.

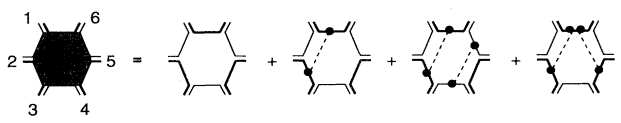

FIG. 5. Diagrams contributing to the interaction of six diffuson propagators: H_6. To 1,3,5 the incoming diffuson propagators are connected, to 2,4,6 the outgoing ones. Possible rotations of the three rightmost diagrams are not drawn; in total there are 16 diagrams.

VI. INFLUENCE OF THE INCOMING BEAM PROFILE

Now that the leading interference processes are known, inserting the diffuson propagators gives the final value of the third cumulant. We first consider the simple case of incoming plane waves. As there can be no transversal momentum difference in the incoming amplitudes, all Q_i

vanish. As a result, all diffuson propagators are simple linear functions of z. We find from Eq. (33)

$$\langle\langle T_a^3\rangle\rangle = \frac{16}{15g^2} = \frac{12}{5}\langle\langle T_a^2\rangle\rangle^2 \qquad \text{(plane wave)},\ \rho_0 \gg L. \tag{34}$$

In practice, however, we deal with a Gaussian beam with limited spot size, influencing the cumulants in two ways. First, if the spot size decreases to values comparable to the sample thickness we have to convolute over a range of incoming momenta, just like we did when calculating the second cumulant. Second, the Gaussian profile brings an extra geometrical factor, as we will show below.

We need the expression when diffuson propagators with an arbitrary momentum are connected to the Hikami boxes. The outgoing diffuson propagators still have no transverse momentum. Because of momentum conservation, the transversal momentum Q_7 of the diffuson propagator connecting the two four-boxes must equal Q_5. The integration over the possible momenta results again in a Gaussian weight function. From the definition (21) we derive

$$\int d^2P_1 d^2P_3 d^2P_5\ \phi(P_1)\phi^*(P_1+Q_1)\ \phi(P_3)\phi^*(P_3+Q_3) \times \phi(P_5)\phi^*(P_5+Q_5) = e^{-\rho_0^2(Q_1^2+Q_3^2+Q_5^2)/8}. \tag{35}$$

Momentum conservation is used to eliminate also Q_5 and reduce the integration to two transversal momenta. The final result for the third cumulant is obtained by inserting the momentum-dependent diffuson propagators into Eq. (33). This gives

$$\begin{aligned}\langle\langle T_a^3\rangle\rangle = \frac{\rho_0^4}{16\pi^2 g^2}\int d^2Q_1 d^2Q_3 \\ \times \exp\left\{-\rho_0^2[Q_1^2+Q_3^2+(Q_1+Q_3)^2]/8\right\} \\ \times F_3(|Q_1|L, |Q_3|L, |Q_1+Q_3|L),\end{aligned} \tag{36}$$

with

$$\begin{aligned}F_3(x_1,x_3,x_5) = \sum_{\text{per}}\Bigg[&\frac{(x_1+x_3)^2 x_5\cosh(x_1+x_3)}{(x_1+x_3+x_5)^2(x_1+x_3-x_5)^2} - \frac{(x_1-x_3)^2 x_5\cosh(x_1-x_3)}{(x_1-x_3+x_5)^2(x_1-x_3-x_5)^2} \\ &- \frac{(x_1+x_3)x_5\sinh(x_1+x_3)}{(x_1+x_3+x_5)(x_1+x_3-x_5)} + \frac{(x_1-x_3)x_5\sinh(x_1-x_3)}{(x_1-x_3+x_5)(x_1-x_3-x_5)} \\ &+ \frac{(x_1+x_3)\cosh(x_1+x_3+2x_5)}{4(x_1+x_3+x_5)^2} - \frac{(x_1+x_3)\cosh(x_1+x_3-2x_5)}{4(x_1+x_3-x_5)^2} \\ &- \frac{(x_1-x_3)\cosh(x_1-x_3+2x_5)}{4(x_1-x_3+x_5)^2} + \frac{(x_1-x_3)\cosh(x_1-x_3-2x_5)}{4(x_1-x_3-x_5)^2}\Bigg] \\ &\times\left[x_5\sinh(x_1)\sinh(x_3)\sinh^2(x_5)\right]^{-1},\end{aligned} \tag{37}$$

which is the main result in this paper. We study again the behavior where the beam diameters are wide. In the limit of large beam diameter ($\rho_0 \gg L$) one finds $F_3(0,0,0) = \frac{16}{15}$; this means for the third cumulant $\langle\langle T_a^3\rangle\rangle = 4F_3(0,0,0)/3g^2$ or

$$\langle\langle T_a^3\rangle\rangle = \frac{16}{5}\,\langle\langle T_a^2\rangle\rangle^2 \qquad \text{(Gaussian profile)},\ \rho_0 \gg L, \tag{38}$$

which differs by a factor $\frac{4}{3}$ from the plane wave limit Eq. (34). This is purely a geometrical effect, depending on the profile of the incoming beam. This effect is best understood in a real space picture. The correlation depends on the distance: it is strongest if the incoming intensities are close. Therefore it is not surprising to see the influence of the overlap. In Ref. [16] this geometrical factor has been calculated for higher orders also (the area of a Gaussian beam is defined differently there). For the experimentally relevant case that the beam diameter is roughly equal to the thickness, we calculated Eqs. (36) and (37) numerically. It then turns out that the behavior of Eq. (38) is actually seen for a large range of beam diameters. The increase of the correlation for smaller beams turns out to be roughly the same for both the third cumulant and the second cumulant squared. All corrections to (38) turn out to be relatively small, as we will discuss below. Apart from this advantage, errors in the sample thickness and the mean free path cancel by presenting the results as the ratio between the second cumulant squared and the third cumulant.

VII. INFLUENCE OF INTERNAL REFLECTION

In this section we calculate the influence of internal reflection on our results and show that it is small. It was seen in previous work [31,27] that surface reflection decreases the C_2 correlation. In Eq. (38) corrections from boundary reflection partly cancel. We did not calculate the influence of internal reflections for the general case, but only for the case of very broad beams (i.e., only for

Q-independent diffuson propagators). One expects that this behavior may be extrapolated to the Q-dependent case. At least for the second cumulant this is a good approximation [27]. The Q-independent diffuson propagators in the presence of internal reflections are [21]

$$\mathcal{L}^a_{\rm in} = \frac{4\pi\tau_1(\mu_a)}{k\ell A\mu_a}\frac{L-z+z_0}{L+2z_0}, \qquad \mathcal{L}_{\rm out}(z) = \frac{k}{\ell}\frac{z+z_0}{L+2z_0}, \tag{39}$$

where z_0 is the extrapolation length. In the definition of g and T_a , we replace L by $L+2z_0$. If internal reflections are absent, $z_0 = 0.71\ell$ and the corrections, which are of order z_0/L, are often negligible. With internal reflection present z_0 increases and should be taken into account [21]. The correlations are known to decrease if internal reflections are present [31,27]. In the first order of z_0/L the second and the third cumulant behave as

$$\langle\langle T_a^2\rangle\rangle = \frac{2}{3g}\left(1-3\frac{z_0}{L}\right),$$
$$\langle\langle T_a^3\rangle\rangle = \frac{16}{15g^2}\left(1-\frac{15}{2}\frac{z_0}{L}\right), \tag{40}$$

Therefore, the central relation (38) has a correction

$$\frac{\langle\langle T_a^3\rangle\rangle}{\langle\langle T_a^2\rangle\rangle^2} = \frac{16}{5}\left(1-\frac{3}{2}\frac{z_0}{L}\right). \tag{41}$$

The experimental determination of the index of refraction of the sample, which determines z_0, is difficult [32]. Fortunately, the correction is rather small for the experimental situation considered.

VIII. CONTRIBUTIONS FROM DISCONNECTED DIAGRAMS

So far the leading contributions to the second and the third cumulants have been calculated. They are given by the connected diagrams in Fig. 2(b) and Figs. 3(c) and 3(d), respectively. Yet there are also contributions to the second and the third cumulants from disconnected diagrams. The diagram in Fig. 2(a) gives an additional contribution to the second cumulant and likewise the diagrams of Figs. 3(a) and 3(b) give a contribution to the third cumulant. These disconnected diagrams correspond to cumulant contributions that are not (fully) due to interference. They describe effects that have little to do with the interference effects we are after. Here we calculate their contribution and show that they are small.

A. Extra contributions to the second cumulant

We first explain the contribution of Fig. 2(a) to the second cumulant. As a start we use the model of a waveguide. We assume that the disorder couples one incoming mode a to all outgoing modes. A waveguide has discrete modes and for the moment we assume that different outgoing modes are uncorrelated. The second moment $\langle T_a^2\rangle$ is split into a connected part $\langle T_a^2\rangle_{\rm con}$ [Fig. 2(b)] and a disconnected part $\langle T_a^2\rangle_{\rm dis}$ [Fig. 2(a)]. The total transmission is the summation over all outgoing modes $T_a = \sum_b T_{ab}$. The disconnected part of the second moment is

$$\begin{aligned}\langle T_a^2\rangle_{\rm dis} &= \sum_{b_1\neq b_2}^{N,N}\langle T_{ab_1}T_{ab_2}\rangle + \sum_{b_1=b_2}^{N}\langle T_{ab_1}T_{ab_2}\rangle \\ &= N(N-1)\langle T_{ab}\rangle^2 + N\langle T_{ab}^2\rangle \\ &= \langle T_a\rangle^2 + N\langle T_{ab}\rangle^2,\end{aligned} \tag{42}$$

where N is the number of modes supported by the waveguide. For the last equality the averaged second moment of the intensity speckle is given by the speckle distribution function Eq. (2), $\langle T_{ab}^2\rangle = 2\langle T_{ab}\rangle^2$. From Eq. (42) we see that the disconnected diagram $\langle T_a^2\rangle_{\rm dis}$ does not completely factorize into the average squared $\langle T_a\rangle^2$. Therefore it contributes to the second cumulant. As shown above, the connected part of the second moment of the total transmission $\langle T_a^2\rangle_{\rm con}$ is proportional to $L/N\ell$. For the sum of the disconnected and the connected contribution to the second cumulant one thus finds

$$\langle\langle T_a^2\rangle\rangle = \langle\langle T_a^2\rangle\rangle_{\rm con} + \langle\langle T_a^2\rangle\rangle_{\rm dis} = \frac{L}{2N\ell} + \frac{1}{N}, \tag{43}$$

which also holds for the plane wave case. After this we turn to the situation of a diffusely scattering slab, with a finite focus of the incoming beam. The incoming beam will be broadened in the transverse direction by diffusion, changing the above result. To calculate the different contributions to the cumulants, for the moment the intensity distribution at the exit interface at transversal coordinates R_1 and R_2 is needed.

The amplitudes, making up each diffuson propagator, can propagate from the outgoing surface in different directions P_1, P_2, P_3, and P_4, respectively,

$$\Psi(R_1)e^{iP_1R_1}\Psi^*(R_1)e^{-iP_2R_1}\Psi(R_2)e^{iP_3R_2}\Psi^*(R_2)e^{-iP_4R_2}. \tag{44}$$

To get the contribution to the second moment of the total transmission, one first integrates over the transversal coordinates R_1 and R_2 to get the contribution of the whole exit interface to the intensity in a certain direction and then one integrates over all directions to get the total transmission. To obtain intensities the amplitudes need to be paired giving the following possibilities. The first possible pairing of the amplitudes is $P_1 = P_2$, $P_3 = P_4$ [see Fig. 6(a)] and brings

$$\int dR_1 \int dR_2\, \langle\Psi(R_1)\Psi^*(R_1)\Psi(R_2)\Psi^*(R_2)\rangle = I^2(0), \tag{45}$$

where we have defined $I(Q)$ as the transmission by a diffuson propagator with transverse momentum Q. Including the incoming Gaussian beam profile, it is proportional

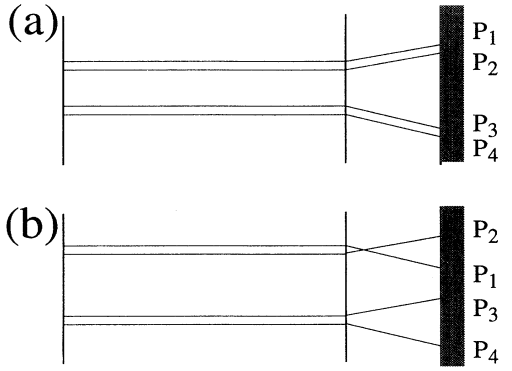

FIG. 6. Disconnected contribution to the second moment. In (a) the two transmissions factorize into the average value squared and do not contribute to the second cumulant. Diagram (b) is much smaller, but gives a contribution to the second cumulant. The amplitudes making up the two diffuson propagators propagate out in different directions.

to [see Eqs. (9) and (21)]

$$I(Q) \propto \frac{|Q|e^{-Q^2\rho_0^2/8}}{\sinh|Q|L}. \tag{46}$$

Integrating over all outgoing directions results in

$$\frac{\langle T_a^2\rangle}{\langle T_a\rangle^2} = \frac{\pi^2k^4I^2(0)}{\pi^2k^4I^2(0)}. \tag{47}$$

This is just the factorizing contribution and hence does not contribute to the second cumulant.

The second possible pairing of the amplitudes $P_1 = P_4$, $P_2 = P_3$ does give a contribution to the second cumulant. It is the diagram in Fig. 6(b),

$$\int dR_1dR_2\ \langle\Psi(R_1)\Psi^*(R_1)\Psi(R_2)\Psi^*(R_2)\rangle e^{iR_1(P_1-P_2)}$$

$$\times e^{-iR_2(P_1-P_2)} = I(P_1-P_2)I(P_2-P_1). \tag{48}$$

Subsequent integration over the outgoing directions P_1 and P_2 yields

$$\langle T_a^2\rangle = \pi k^2\int_{|Q|<k} d^2Q\ I^2(Q). \tag{49}$$

The integral can be extended to infinity since $I(Q)$ is an exponentially decaying function. The contribution of the disconnected diagram Fig. 2(b) to the second cumulant is thus

$$\langle\langle T_a^2\rangle\rangle_{\rm dis} = \frac{\pi k^2\int_{-\infty}^{\infty} d^2QI^2(Q)}{\pi^2k^4I^2(0)} \equiv \frac{1}{N}. \tag{50}$$

In analogy to the waveguide, this result describes irreducible contributions from disconnected diagrams. It can be interpreted as the inverse of the number of independent speckle spots in transmission at the exit interface [33,15].

B. Extra contributions to the third cumulant

We apply the same method for contributions to the third cumulant. Following the waveguide argument as above, we find the contributions to the third cumulant of the diagrams of Figs. 3(c) and 3(d), 3(b), and 3(a), respectively,

$$\langle\langle T_a^3\rangle\rangle = \frac{3}{5}\frac{L^2}{N^2\ell^2} + \frac{6}{2}\frac{L}{N^2\ell} + \frac{2}{N^2}. \tag{51}$$

The first term on the right-hand side is the connected diagram. It is clear that the second term, the diagram of Fig. 3(b), gives a much larger contribution to the third cumulant than the third term, the diagram of Fig. 3(a), as the diagram Fig. 3(b) is already enhanced by some interference. In the following we consider only the diagram of Fig. 3(b).

As can be seen from Fig. 3(b), there are three possibilities to combine the three diffuson propagators into two connected diffuson propagators and a single diffuson propagator. Attaching outgoing directions to the amplitudes at the exit interface gives (see Fig. 7),

$$\Psi(R_1)e^{iP_1R_1}\Psi^*(R_1)e^{-iP_2R_1}\Psi(R_2)e^{iP_3R_2}\Psi^*(R_2)$$

$$\times e^{-iP_4R_2}\Psi(R_3)e^{iP_5R_3}\Psi^*(R_3)e^{-iP_6R_3}. \tag{52}$$

It is clear that there are six possibilities to pair the outgoing directions into intensities. Integrating over the transversal coordinates R_1, R_2, and R_3 gives six contributions

$$\begin{aligned} &I_{\rm con}(0)I_{\rm con}(0)I(0),\\ &I_{\rm con}(P_1-P_3)I_{\rm con}(P_3-P_1)I(0),\\ &I_{\rm con}(0)I_{\rm con}(P_1-P_5)I(P_5-P_1),\\ &I_{\rm con}(0)I_{\rm con}(P_3-P_5)I(P_5-P_3),\\ &I_{\rm con}(P_1-P_5)I_{\rm con}(P_3-P_1)I(P_5-P_3),\\ &I_{\rm con}(P_1-P_3)I_{\rm con}(P_3-P_5)I(P_5-P_1)\,, \end{aligned} \tag{53}$$

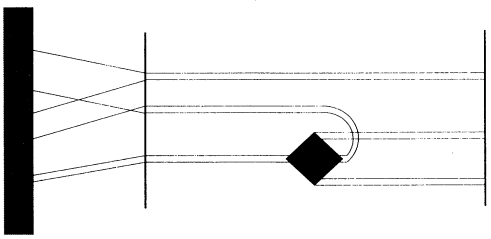

FIG. 7. Leading disconnected contribution to the third cumulant; the box symbolizes again the Hikami vertex.

where $I_{\rm con}$ denotes the transmitted intensity coming from the connected part of Fig. 3(b). The third cumulant is in the discrete mode model given by

$$\langle\langle T_a^3\rangle\rangle = \frac{1}{\langle T_a\rangle^3}\left[\sum_{b,b',b''}\langle T_{ab}T_{ab'}T_{ab''}\rangle - 3\sum_b\langle T_{ab}\rangle\sum_{b,b'}\langle T_{ab}T_{ab'}\rangle + 2\sum_b\langle T_{ab}\rangle^3\right]. \quad (54)$$

Similarly to the second cumulant we insert all pairings of Eq. (53) and find for the contribution from disconnected diagrams

$$\langle\langle T_a^3\rangle\rangle_{\rm dis} = \frac{6}{\langle T_a\rangle^3}\int d^2Q_1 d^2Q_2 d^2Q_3 \times[I_{\rm con}(0)I_{\rm con}(Q_1)I(-Q_1) + I_{\rm con}(Q_1)I_{\rm con}(Q_2)I(Q_3)]. \quad (55)$$

The integrand is dominated by its first term, which is depicted in Fig. 7. We explicitly evaluate this term. The calculation follows completely the line of the second cumulant calculation, yet it is slightly more complicated as it has a Q-dependent outgoing diffuson propagator. The integration over Q_2 and Q_3 gives a factor $(\pi k^2)^2$. Comparing the result with the last two terms in the third cumulant in the waveguide model Eq. (51), we define N^* as

$$\langle\langle T_a^3\rangle\rangle_{\rm dis} = 6\langle\langle T_a^2\rangle\rangle_{\rm con}/N^*. \quad (56)$$

The number N^* is inversely proportional to the contribution of disconnected diagrams to the third cumulant for a Gaussian profile.

C. Polarization effects

The vector character of the light has not been taken into account yet. The two independent polarizations of each outgoing direction effectively double the number of independent speckle spots N. Thus, for an incoming plane wave of unit intensity with fixed polarization the total transmission and the conductance g are twice as large as they would be in the scalar case. As we work with normalized cumulants, this effect reduces only the value of the second cumulant ($\propto 1/g$) and the value of the third cumulant ($\propto 1/g^2$). Therefore, it is immediately seen that the relation $\langle\langle T_a^3\rangle\rangle \propto \langle\langle T_a^2\rangle\rangle^2$ [Eq. (38)] is not affected. The vector character does reduce the correction Eq. (50) by a factor 2. For the experimental data of Ref. [15] the number of modes N as well as N^* is listed in Table I (including the doubling).

Summarizing the previous sections we have included three corrections. We first obtained the result for very broad Gaussian beams, in the large L/ℓ limit, Eq. (38). The first correction was the influence of a finite beam diameter, which changes the diffuse intensity from linear into an exponentially decaying; see Eq. (9). This correction is contained in Eqs. (37) and (36). The presence of internal reflections also changes the spatial dependence of the diffuse intensity resulting in a correction Eq. (41). The third correction is of another nature; it is the only process that does not come from interference, but from disconnected diagrams. Only this term depends on the number of modes, which in the vector case is twice as large as in the scalar case.

IX. COMPARISON WITH EXPERIMENTS

The data set found experimentally in Ref. [15] are reproduced in Table I and Fig. 8. The experiments reported there were performed with seven different samples. The experimental setup and measurement technique used is extensively described in Ref. [8]. Samples consisted of 36 vol% rutile TiO_2 pigment on a transparent substrate. The extrapolation length was estimated from the effective index of refraction to be $z_0 \approx 1.1$ μm. The absorption length ℓ_a was determined to be $\simeq 70$ μm.

TABLE I. Sample thickness, beam width, second cumulant, and third cumulant for the different samples as taken from Ref. [15]. Next are the beam diameter correction factor on the third cumulant (see Sec. IX) and the number of modes N and N^*. Together they give the corrected (plotted) cumulants (last two columns).

Sample thickness L (μm)	Beam diameter ρ_0 (μm)	Second cumulant (units of 10^{-4})	Third cumulant (units of 10^{-7})	Beam diameter correction	Number of modes N	Number of modes N^*	Corrected second cumulant (units of 10^{-4})	Corrected third cumulant (units of 10^{-7})
30	77	0.36±0.01	0.014 ±0.035	1.03	388000	300000	0.33	0.007
12	26	0.97 ±0.03	−0.03 ±0.25	1.04	46800	36800	0.75	−0.18
22	32	1.24 ±0.04	0.68 ±0.28	1.06	88600	72100	1.13	0.58
30	33	1.57 ±0.04	1.30 ±0.46	1.07	119000	99300	1.49	1.21
53	35	1.80 ±0.03	0.91 ±0.53	1.10	241000	212000	1.76	0.86
30	26	1.90 ±0.03	0.92 ±0.56	1.09	94900	81300	1.79	0.78
45	33	1.90 ±0.05	1.33 ±0.43	1.10	187000	163000	1.84	1.26
53	26	2.18 ±0.03	1.77 ±0.59	1.10	208000	189000	2.13	1.70
170	27	2.69 ±0.06	2.02 ±0.82	1.13	1420000	1430000	2.68	2.00
78	28	2.74 ±0.03	2.43 ±0.62	1.11	396000	372000	2.71	2.39
30	17	4.82 ±0.10	9.1 ±3.3	1.11	71900	64400	4.68	8.60
30	10	8.01 ±0.36	5.3 ±6.4	1.11	60200	56400	7.84	4.47

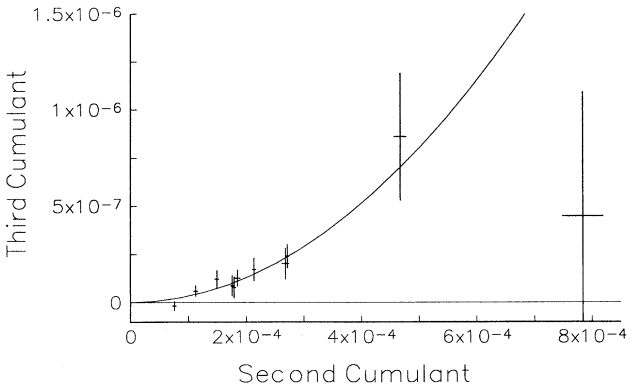

FIG. 8. Third cumulant plotted against the second cumulant. The points are the corrected experimental data (see the text). The line is the theoretical prediction $\langle\langle T_a^3\rangle\rangle = 3.2\langle\langle T_a^2\rangle\rangle$; no free parameters were introduced.

Different values of the conductance g were probed by taking various sample thicknesses and by varying the beam diameter. The fluctuations in the total transmission were measured by varying the wavelength of the light.

For a very broad beam we found the simple relation (38) between the second and the third cumulant. A weighted least-squares fit to

$$\langle\langle T_a^3\rangle\rangle = \text{const} \times \langle\langle T_a^2\rangle\rangle^2 \tag{57}$$

of the raw experimental data yields a prefactor 2.9 ± 0.6. However, as discussed above, there are three corrections to be made. First, if the beam width becomes comparable to sample thickness, the integrals (23) and (36) have to be performed: If the beam width reduces, g decreases accordingly and both cumulants increase in absolute size. Yet the precise increase is somewhat different, resulting in a somewhat smaller prefactor in Eq. (38). We corrected each data point individually for its finite focus, mapping it to the infinite focus case. The third cumulant was multiplied by a factor that ranged from 1.03 to 1.13 as L/ρ_0 ranged from 0.41 to 6.3; see Table I. This is the largest correction, which changes the prefactor some 10%. Second, we corrected for internal reflections according to Eq. (41). The third correction comes from the disconnected diagrams. The contributions from the disconnected diagrams are substracted from the measured cumulants. After all these corrections the data should again obey the law $\langle\langle T_a^3\rangle\rangle = 3.2\,\langle\langle T_a^2\rangle\rangle^2$. The results are plotted in Fig. 8, where the points are the corrected data points and the line is the theoretical prediction. A least-squares fit gives

$$\langle\langle T_a^3\rangle\rangle = (3.3 \pm 0.6)\langle\langle T_a^2\rangle\rangle^2. \tag{58}$$

Note that there is no adjustable parameter. We find that there is good agreement between experiment and theory. All corrections are minor as compared to the error in the data; fitting the raw data is also in agreement with the theoretical value of 3.2. We recall that the major shift between fits of raw and corrected data comes from the beam diameter correction. Inspecting Fig. 8 one might be tempted to make a linear fit, but in Ref. [15] it was shown that this fit is statistically improbable.

X. DISCUSSION

We have calculated the second and the third cumulants of the distribution of the total transmission underlying the conclusions of Ref. [15] and compared it to the experimental data. Both cumulants are a consequence of interference between diffuse channels. They were calculated with a diagrammatic technique. The inverse dimensionless conductance, interpreted as an interference probability, is a perturbation parameter in the theory. The third cumulant is proportional to the second cumulant squared. We also found a nontrivial dependence on the profile of the incoming beam used. The cumulants were calculated for arbitrary beam diameter, but the influence of a finite focus on the ratio is rather weak. Also boundary reflections were included. Our calculations confirm that the main contributions come from diagrams with interference processes, i.e., connected diagrams, as we have shown that the contributions from disconnected diagrams is small. The experimentally found ratio of the third cumulant versus the second cumulant squared is well described by our theory.

The extension of the calculations to higher cumulants is straightforward. The nth cumulant will contain $(n-1)$ Hikami four-point vertices. So the contribution is estimated to be $\langle\langle T_a^n\rangle\rangle \propto g^{1-n}$. Also corrections and cancellations from higher-order vertices are present, but it is clear that the calculation becomes laborious at large n. Recently two of the authors discovered that all the cumulants of the distribution function can be mapped onto the moments of the eigenvalue distribution of the transmission matrix [16]. The eigenvalue distribution is bimodal and was first calculated using random matrix techniques [34], but recently its validity beyond quasi-one-dimension was proven [35]. As the eigenvalue distribution is known, the entire distribution of the total transmission was calculated in the limit of broad beams. These results agree with calculations presented here for the first three cumulants. The experimental data thus also prove the first few moments of the eigenvalue distribution function. As only three moments are known, it is impossible to reconstruct the full eigenvalue distribution from the experimental data. The present calculation leads us to assume that the eigenvalue distribution in a diagrammatic approach is also given by loopless connected diagrams. As the ratio of first few cumulants does not depend sensitively on the beam diameter, the results of Ref. [16] are probably also valid in the regime where the beam diameter becomes comparable to the sample thickness.

ACKNOWLEDGMENTS

The authors thank E. Kogan and C. W. J. Beenakker for discussion. This work was partly supported by the Stichting vor Fundamenteel Onderzoek der Materie, which is a part of the Nederlandse Organisatie voor Wetenschappelijk Onderzoek. The research of Th. M. N. was supported by the Royal Netherlands Academy of Arts and Sciences and also sponsored by NATO (Grant No. CGR 921399).

[1] Y. Kuga and A. Ishimaru, J. Opt. Soc. Am. A **1**, 831 (1985).
[2] M. P. van Albada and A. Lagendijk, Phys. Rev. Lett. **55**, 2692 (1985).
[3] P. Wolf and G. Maret, Phys. Rev. Lett. **55**, 2696 (1985).
[4] M. J. Stephen and G. Cwilich, Phys. Rev. Lett. **59**, 285 (1987).
[5] B. Shapiro, Phys. Rev. Lett. **57**, 2168 (1986).
[6] S. Feng, C. Kane, P. Lee, and A. D. Stone, Phys. Rev. Lett. **61**, 834 (1988).
[7] N. Garcia, A. Z. Genack, R. Pnini, and B. Shapiro, Phys. Lett. A **176**, 458 (1993).
[8] J. F. de Boer, M. P. van Albada, and A. Lagendijk, Phys. Rev. B **45**, 658 (1992).
[9] B. L. Altshuler, Pis'ma Zh. Eksp. Teor. Fiz. **41**, 530 (1985) [JETP Lett. **41**, 649 (1985)].
[10] P. A. Lee and A. D. Stone, Phys. Rev. Lett. **55**, 1622 (1985).
[11] P. A. Lee, A. D. Stone, and H. Fukuyama, Phys. Rev. B **35**, 1039 (1987).
[12] A. Z. Genack and N. Garcia, Europhys. Lett. **21**, 753 (1993).
[13] E. Kogan, M. Kaveh, R. Baumgartner, and R. Berkovits, Phys. Rev. B **48**, 9404 (1993).
[14] B. L. Altshuler, V. E. Kravtsov, and I. V. Lerner, in *Modern Problems in Condensed Matter Sciences*, edited by B. L. Altshuler, P. A. Lee, and R. A. Webb (North-Holland, Amsterdam, 1991), Vol. 30, p. 449.
[15] J. F. de Boer *et al.*, Phys. Rev. Lett. **73**, 2567 (1994).
[16] Th. M. Nieuwenhuizen and M. C. W. van Rossum, Phys. Rev. Lett. **74**, 2674 (1995).
[17] J. R. Gao *et al.* (unpublished).
[18] A. M. S. Macêdo, Phys. Rev. B **49**, 1858 (1994).
[19] I. Edrei, M. Kaveh, and B. Shapiro, Phys. Rev. Lett. **62**, 2120 (1989).
[20] H. C. van de Hulst, *Multiple Light Scattering, Vols. 1 and 2* (Academic, New York, 1980).
[21] Th. M. Nieuwenhuizen and J. M. Luck, Phys. Rev. E **48**, 560 (1993).
[22] M. C. W. van Rossum, Th. M. Nieuwenhuizen, and R. Vlaming, Phys. Rev. E **51**, 6158 (1995).
[23] R. Pnini and B. Shapiro, Phys. Rev. B **39**, 6986 (1989).
[24] B. Z. Spivak and A. Y. Zyuzin, Solid State Commun. **65**, 311 (1988).
[25] R. Berkovits and S. Feng, Phys. Rep. **238**, 135 (1994).
[26] M. P. van Albada, J. F. de Boer, and A. Lagendijk, Phys. Rev. Lett. **64**, 2787 (1990).
[27] M. C. W. van Rossum and Th. M. Nieuwenhuizen, Phys. Lett. A **177**, 452 (1993).
[28] S. Hikami, Phys. Rev. B **24**, 2671 (1981).
[29] Th. M. Nieuwenhuizen and M. C. W. van Rossum, Phys. Lett. A **177**, 102 (1993).
[30] L. P. Gor'kov, A. I. Larkin, and D. Khmel'nitskii, Pis'ma Zh. Eksp. Teor. Fiz. **30**, 248 (1979) [JETP Lett. **30**, 228 (1979)].
[31] A. A. Lisyansky and D. Livdan, Phys. Lett. A **170**, 53 (1992).
[32] P. N. den Outer and A. Lagendijk, Opt. Commun. **103**, 169 (1993).
[33] J. W. Goodman, in *Laser Speckle and Related Phenomena*, edited by J. C. Dainty (Springer, Berlin, 1975), Vol. 9, p. 9.
[34] O. N. Dorokhov, Solid State Commun. **51**, 381 (1984).
[35] Yu. V. Nazarov, Phys. Rev. Lett. **73**, 134 (1994).